Wind-Driven Formation of Ice Bridges in Straits

Bhargav Rallabandi,[1] Zhong Zheng,[1] Michael Winton,[2] and Howard A. Stone[1,*]
[1]Department of Mechanical and Aerospace Engineering, Princeton University, Princeton, New Jersey 08544, USA
[2]NOAA/Geophysical Fluid Dynamics Laboratory, Princeton, New Jersey 08542, USA
(Received 26 September 2016; published 21 March 2017)

Ice bridges are static structures composed of tightly packed sea ice that can form during the course of its flow through a narrow strait. Despite their important role in local ecology and climate, the formation and breakup of ice bridges is not well understood and has proved difficult to predict. Using long-wave approximations and a continuum description of sea ice dynamics, we develop a one-dimensional theory for the wind-driven formation of ice bridges in narrow straits, which is verified against direct numerical simulations. We show that for a given wind stress and minimum and maximum channel widths, a steady-state ice bridge can only form beyond a critical value of the thickness and the compactness of the ice field. The theory also makes quantitative predictions for ice fluxes, which are particularly useful to estimate the ice export associated with the breakup of ice bridges. We note that similar ideas are applicable to dense granular flows in confined geometries.

DOI: 10.1103/PhysRevLett.118.128701

An ice bridge is a stationary rigid structure composed of sea ice, which spans the width of a strait between two land masses, usually separated by a static arch from a large region of open water (a polynya). Such ice bridges are formed seasonally in many of the straits and channels in the Canadian Arctic Archipelago (usually in the narrowest part of the strait), persisting for several months and impacting local climate and ecology [1,2]. Once formed, an ice bridge controls the edge of the main ice pack (e.g., in Nares Strait), thus inhibiting the flow and subsequent loss of Arctic sea ice into warmer oceans and potentially influencing global climate [3]. Further, the polynya itself plays a key role in regulating the uptake of solar energy and the transport of gases and nutrients that are crucial for the sustenance of marine food chains [4,5]. Despite their seasonal occurrence and biogeophysical importance, the conditions under which ice bridges form are not well understood.

Here, we develop a theoretical framework to describe the wind-driven flow of sea ice through a narrow channel, focusing on ice bridge formation. The methods used here to describe ice bridge formation, because of the rheological description of the ice flow, are more broadly applicable to flows of granular media and other complex materials. We consider the motion of sea ice in a symmetric channel of arbitrary shape, $y = w(x)$, with a characteristic half-width w_0 and length $\ell_0 \gg w_0$, as indicated in Fig. 1; typical values are $w_0 \approx 30$ km and $\ell_0 \approx 200$ km. The flow of the ice is driven by an external wind stress $\mathbf{f}$ (typically ~ 0.1 Pa) acting on its top surface, cf. Fig. 1(a), and is impeded by water drag on its bottom surface as well as internal stresses that arise due to a resistance to motion relative to the channel walls [6].

Adopting the widely used approach in climate modeling, we treat the ice field as a 2D continuum rather than considering the dynamics of individual floes. The inertia of the ice is negligible on time scales longer than a few hours, and water drag, being quadratic in the relative ice-ocean velocity, is small relative to other stress terms for slowly moving ice and weak ocean currents [6,7]. The Coriolis force is an order of magnitude smaller than wind stress for a typical ice velocity ($\sim 0.1\ \mathrm{m\,s^{-1}}$) and thickness ($\sim 1$ m) and is smaller still for stationary (bridged) ice. Thus, at first approximation, the depth-integrated stress equation reduces to the two-dimensional balance [6,8,9]

$$\nabla \cdot \boldsymbol{\sigma} + \mathbf{f} = \mathbf{0}, \tag{1}$$

where $\boldsymbol{\sigma}(x, y, t)$ is the depth-integrated internal stress tensor (units of force per length) associated with the velocity field $\mathbf{u}(x, y, t) = u\mathbf{e}_x + v\mathbf{e}_y$. The surface wind stress $\mathbf{f}$ has units of force per area and is assumed to be a constant and unidirectional for simplicity, i.e., $\mathbf{f} = f\mathbf{e}_x$. Water stress, which is necessary to establish free drift of the ice, can be

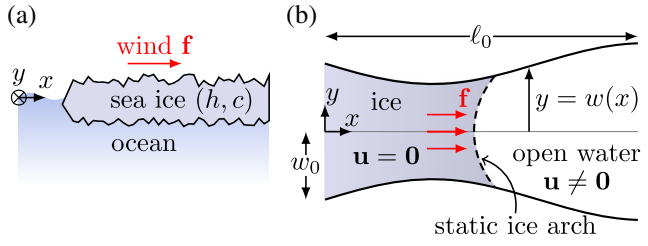

FIG. 1. Schematic of the setup and forcing conditions, indicating the coordinate system and the external wind stress. Panel (a) shows a section normal to the plane of flow, and (b) sketches a plan view of the narrow channel geometry with $\ell_0 \gg w_0$, indicating the possible formation of a static ice arch. The ice field is described using an effective thickness h and a compactness c.

included in the theory that we develop here, but does not significantly affect ice-bridge formation.

We use Hibler's viscous-plastic constitutive law for sea ice [10,11], in which $\boldsymbol{\sigma}$ is related to the rate-of-strain tensor $\mathbf{E} = \frac{1}{2}(\nabla\mathbf{u} + \nabla\mathbf{u}^T)$ by

$$\boldsymbol{\sigma} = -p\mathbf{I} + \eta(\alpha^2 - 1)(\mathrm{tr}\mathbf{E})\mathbf{I} + 2\eta\mathbf{E}, \tag{2}$$

where α is an $\mathcal{O}(1)$ parameter that represents the eccentricity of an elliptic yield curve, and p is the depth-integrated average normal stress (also referred to as a pressure). The depth-integrated viscosity η depends on both p and $\mathbf{E}$ and is given by the relation

$$\eta = \frac{1}{\alpha^2}\max\left(\frac{p}{E}, \zeta_{\min}\right), \tag{3}$$

where $E \equiv \alpha^{-1}\sqrt{2\mathrm{tr}(\mathbf{E}\cdot\mathbf{E}) + (\alpha^2 - 1)(\mathrm{tr}\mathbf{E})^2}$ is a measure of the strain rate. Thus, the rheology is nominally plastic (i.e., $\boldsymbol{\sigma}$ is invariant to a rescaling of $\mathbf{E}$ for $\eta = \alpha^{-2}p/E$), with a viscous regularization for large strain rates ($\eta = \alpha^{-2}\zeta_{\min}$ for $E > p/\zeta_{\min}$) [12]. The dependence of η on p and E shares several similarities with continuum models of dense granular flows [13–15]; hence, the results we derive below should be widely applicable.

The sea ice thickness distribution [16,17] is approximated by a two-level model: the effective thickness h is defined as the ice mass per unit area divided by its density (assumed constant) and the compactness c, as the area fraction of rheologically active "thick" ice relative to the total area covered by ice (including open water) [11]. Neglecting thermodynamic sources of thickness redistribution (e.g., precipitation and phase changes), the conservation equations for h and c are [11]

$$\frac{\partial h}{\partial t} + \nabla\cdot(\mathbf{u}h) = 0 \quad \text{and} \tag{4a}$$

$$\frac{\partial c}{\partial t} + \nabla\cdot(\mathbf{u}c) = 0, \quad \text{with} \quad 0 \le c \le 1. \tag{4b}$$

Since the pressure p is a depth-integrated stress, it is linearly related to h to good approximation [6,18,19]. On the other hand, p decreases strongly for c not close to unity (due to decreased interactions between floes), motivating a relationship of the form

$$p = She^{-k(1-c)}, \tag{5}$$

where S is a strength constant (with units of force per area), and k is a dimensionless model parameter [11]. Equations (1)–(5) define Hibler's sea ice model [11], and form a coupled system for the unknowns $\mathbf{u}$, h, c, η, and p (functions of x, y and t) in terms of parameters α, $\zeta_{\min}$, S, and k. The system can be solved subject to initial conditions on h and c, and the no-slip condition at the channel walls $\mathbf{u}|_{y=\pm w(x)} = \mathbf{0}$.

The standard approach in climate modeling with sea ice is to treat this nonlinear problem numerically [6,8,20]. Here, we obtain analytical results that are applicable when a strait is narrow, i.e., $\delta \equiv w_0/\ell_0 \ll 1$, by first developing an approximate expression for the ice velocity as a function of p and the channel shape $w(x)$. We then use this result in the continuity equations (4a) and (4b) to obtain reduced-order evolution equations for h and c that admit solutions consistent with ice bridge formation.

Guided by long-wave approximations for plastic flows in channels [21,22], we define dimensionless variables as

$$x = \ell_0\tilde{x}, \quad y = w_0\tilde{y}, \quad u = u_0\tilde{u}, \quad v = \delta u_0\tilde{v},$$
$$t = \frac{\ell_0}{u_0}\tilde{t}, \quad p = p_0\tilde{p}, \quad \eta = \frac{\zeta_{\min}}{\alpha^2}\tilde{\eta}, \quad h = \frac{p_0}{S}\tilde{h}, \tag{6}$$

where u_0 and p_0 are, respectively, characteristic velocity and pressure scales that are to be determined. We note that (5) rescales to become $\tilde{p} = \tilde{h}e^{-k(1-c)}$. Striking a balance between wind stress and transverse shear stress gradients in (1)–(2) yields the velocity scale $u_0 = \alpha^2 w_0^2 f/\zeta_{\min}$. Further, the no-slip condition at the walls demands that the flow behaves viscously ($\eta = \zeta_{\min}/\alpha^2$) near the channel walls, which is realized only when $p \le E\zeta_{\min}$, cf. (3). This latter condition establishes a pressure scale $p_0 = \zeta_{\min}u_0/(\alpha w_0) = \alpha w_0 f$.

Defining $\tilde{E} \equiv E\alpha w_0/u_0$, we can then write

$$\tilde{\eta} = \max\left(\frac{\tilde{p}}{\tilde{E}}, 1\right), \tag{7a}$$

$$\text{with} \quad \tilde{E} = \left|\frac{\partial\tilde{u}}{\partial\tilde{y}}\right| + \mathcal{O}(\delta). \tag{7b}$$

The stress balance (1)–(3), for $\delta \ll 1$, reduces to

$$\frac{\partial\tilde{p}}{\partial\tilde{y}} = 0, \tag{8a}$$

$$\frac{\partial}{\partial\tilde{y}}\left[\tilde{\eta}\left(\frac{\partial\tilde{u}}{\partial\tilde{y}}\right)\right] + 1 = 0, \tag{8b}$$

In contrast with viscous fluid flow in narrow channels, normal and shear stresses in the ice are comparable due to the dependence of $\tilde{\eta}$ on $\tilde{p}$ and E, cf. (2) and (3). Consequently, the longitudinal pressure gradient is an $\mathcal{O}(w_0/\ell_0)$ smaller than the transverse gradient of shear stress and is therefore absent from (8b) at first approximation.

Integrating (8) with respect to $\tilde{y}$ and applying the condition of zero shear stress at the symmetry axis $\tilde{y} = 0$ results in $\tilde{\eta}(\partial\tilde{u}/\partial\tilde{y}) = -\tilde{y}$ and $\tilde{p} = \tilde{p}(\tilde{x}, \tilde{t})$. We recognize that the flow must be viscous ($\tilde{\eta} = 1$) in a layer near the channel walls in order to satisfy the no-slip condition. Within this layer, the expression for shear stress can be integrated subject to the no-slip condition to obtain the velocity $\tilde{u}_v$ in the viscous layer as

$$\tilde{u}_v(\tilde{x}, \tilde{y}, \tilde{t}) = \frac{1}{2}(\tilde{w}^2 - \tilde{y}^2). \tag{9}$$

Observing that $\tilde{\eta} = 1$ is only realized if $\tilde{E} > \tilde{p}$, and that $\tilde{E} \sim |\partial\tilde{u}/\partial\tilde{y}| \sim |\tilde{y}|$ by (7) and (9), we deduce that the viscous layer spans the region $\tilde{p}(\tilde{x}, \tilde{t}) < |\tilde{y}| < \tilde{w}(\tilde{x})$, as sketched in Fig. 2(a).

In the central part of the channel, where $|\tilde{y}| < \tilde{p}(\tilde{x}, t)$, the flow is plastic ($\tilde{\eta} = \tilde{p}/\tilde{E}$) as per (7a). Here, the horizontal velocity is nearly independent of $\tilde{y}$ and can be written as $\tilde{u} \sim \tilde{u}_p(\tilde{x}, \tilde{t})$, see Fig. 2(a). Continuity of velocity across the boundary $|\tilde{y}| = \tilde{p}(\tilde{x}, \tilde{t})$ between the viscous and plastic regions of the flow yields

$$\tilde{u}_p(\tilde{x}, \tilde{t}) = \frac{1}{2}(\tilde{w}^2 - \tilde{p}^2). \tag{10}$$

A singular perturbation analysis shows that $\tilde{\eta} = \mathcal{O}(\delta^{-1})$ and $\partial\tilde{u}/\partial\tilde{y} = \mathcal{O}(\delta)$ in the plastic region [21]; we do not, however, discuss these details here.

Thus, the curves $\tilde{y} = \pm\tilde{p}(\tilde{x}, \tilde{t})$ represent pseudoyield surfaces across which the rheology transitions from plastic to viscous flow. However, if $\tilde{p} > \tilde{w}$ (at some $\tilde{x}$ and $\tilde{t}$), the pseudoyield surface lies "outside" the channel, preventing this transition from occurring and thereby causing the flow to be locally unyielded with $\tilde{u} = 0$, see Fig. 2(a). The different flow behaviors can be combined into a compact expression for $\tilde{u}$:

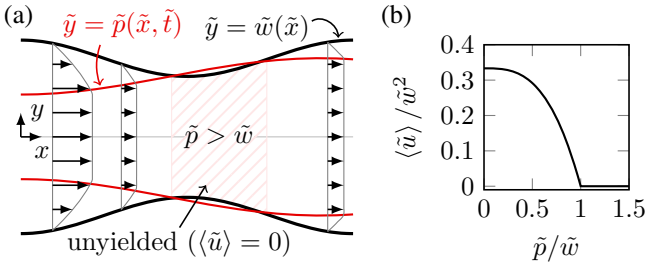

FIG. 2. (a) Velocity profile for a channel of shape $\tilde{w}(\tilde{x})$ with some pressure distribution $\tilde{p}(\tilde{x}, \tilde{t})$. The curves $|\tilde{y}| = \tilde{p}(\tilde{x}, \tilde{t})$ represent pseudoyield surfaces between viscous and plastic flow regions. The ice is unyielded and is locally stationary in parts of the channel where $\tilde{p} > \tilde{w}$ (shaded). (b) Mean velocity $\langle\tilde{u}\rangle$ as a function of $\tilde{p}/\tilde{w}$, as per (12), showing that $\langle\tilde{u}\rangle = 0$ for $\tilde{p}/\tilde{w} > 1$.

$$\tilde{u}(\tilde{x}, \tilde{y}, \tilde{t}) = \max\left\{\frac{1}{2}(\tilde{w}^2 - \max\{\tilde{p}, \tilde{y}\}^2), 0\right\}, \tag{11}$$

which is indicated by arrows in Fig. 2(a). The width-averaged mean flow speed $\langle\tilde{u}\rangle(\tilde{x}, \tilde{t})$ is then

$$\langle\tilde{u}\rangle \equiv \frac{1}{2\tilde{w}}\int_{-\tilde{w}}^{\tilde{w}} \tilde{u}\mathrm{d}\tilde{y} = \max\left\{\frac{\tilde{w}^2}{3}\left(1 - \frac{\tilde{p}^3}{\tilde{w}^3}\right), 0\right\} \tag{12}$$

and is plotted in Fig. 2(b). Thus, a critical condition for flow $\tilde{p} < \tilde{w}$ emerges from the long-wave theory.

We now turn to the continuity equations (4). If $\tilde{h}$ and c are nearly uniform across the channel (contingent on initial conditions), (4) can be integrated across the channel width to eliminate $\tilde{v}$ and obtain averaged 1D equations:

$$\frac{\partial(\tilde{w}\,\tilde{h})}{\partial\tilde{t}} + \frac{\partial(\tilde{w}\langle\tilde{u}\rangle\tilde{h})}{\partial\tilde{x}} = 0 \quad \text{and} \tag{13a}$$

$$\frac{\partial(\tilde{w}c)}{\partial\tilde{t}} + \frac{\partial(\tilde{w}\langle\tilde{u}\rangle c)}{\partial\tilde{x}} = 0, \qquad 0 \le c \le 1. \tag{13b}$$

Equations (12)–(13) form a reduced-order (1D) system of hyperbolic conservation laws for $\tilde{h}(\tilde{x}, \tilde{t})$ and $c(\tilde{x}, \tilde{t})$, coupled through the mean flow speed $\langle\tilde{u}\rangle$; we recall that $\tilde{p} = \tilde{h}e^{-k(1-c)}$. We solve this coupled system numerically using the HLL (Harten–Lax–van Leer) method [23] in which wave information is advanced along local characteristics (see also [24]). As representative examples, we focus here on a uniform initial ice field with $\tilde{h}|_{\tilde{t}=0} = \tilde{h}_i$ and $c|_{\tilde{t}=0} = c_i$ in a channel of nonuniform shape $\tilde{w}(\tilde{x})$. Because of (5), the initial pressure field is also uniform, i.e., $\tilde{p}|_{\tilde{t}=0} = \tilde{p}_i = \tilde{h}_i e^{-k(1-c_i)}$. We hold $\tilde{h} = \tilde{h}_i$ and $c = c_i$ at both the inlet ($\tilde{x} = 0$) and the outlet ($\tilde{x} = 1$); note that the inlet condition amounts to constant fluxes of $\tilde{h}$ and c into the channel.

Figure 3 shows the numerically computed time evolution of the thickness distribution along the channel for two different $\tilde{h}_i$, with $c_i = 1$. The results in Fig. 3(a) correspond to a flow with $\tilde{p}_i < \tilde{w}$ everywhere. In this case, the system evolves towards a steady state characterized by a smooth distribution of ice properties along the channel without bridge formation ($\langle\tilde{u}\rangle > 0$ everywhere).

By contrast, Fig. 3(b) corresponds to a situation in which $\tilde{p}_i > \tilde{w}$ in a part of the channel (region between dashed lines) constituting a local blockage with $\langle\tilde{u}\rangle = 0$, cf. (12). The ice downstream of the blockage flows in response to the wind stress, leaving ever thinning ice in its place, while the incoming ice upstream of the initial blockage piles up until it becomes thick enough to stop flowing. This results in the development of a discontinuity in ice properties that separates thick, compact, and stationary ice from flowing open water ($\tilde{h} = c = 0$), as indicated in Fig. 3(b) and sketched schematically in Fig. 3(c). These results are

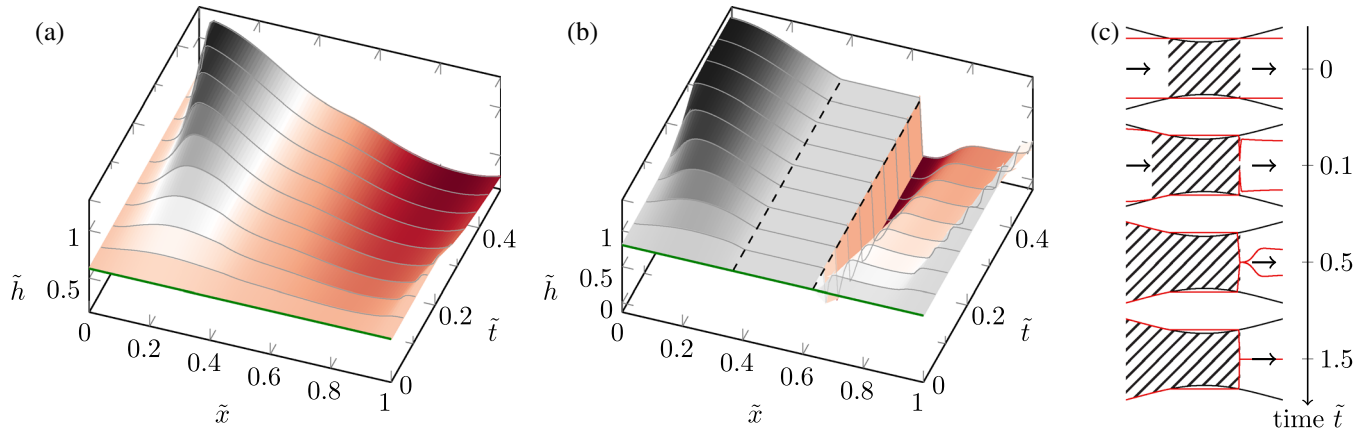

FIG. 3. Time evolution of the reduced-order system (13), computed numerically, in a channel of shape $\tilde{w}(\tilde{x}) = 1 + 0.3\cos 2\pi\tilde{x}$, with uniform initial conditions $\tilde{h}|_{\tilde{t}=0} = \tilde{h}_i$ (green line) and $c|_{\tilde{t}=0} = c_i = 1$. Colors in (a),(b) indicate thinner (red) or thicker (gray) ice, and gray lines are distributions of $\tilde{h}$ along the channel at different $\tilde{t}$. Panel (a) corresponds to $\tilde{h}_i = 0.6$ ($\tilde{p}_i < \tilde{w}$ everywhere), in which the ice field evolves to a flowing state with no bridge formation. Panel (b) corresponds to $\tilde{h}_i = 0.8$, for which $\tilde{p}_i > \tilde{w}$ between the dashed lines, constituting an initial blockage. Ice upstream of the blockage thickens, while ice downstream of the blockage thins, resulting in a 1D realization of an ice arch that separates immobile ice from open water. This process is sketched in (c), which depicts the pseudoyield surfaces $\tilde{y} = \pm\tilde{p}(\tilde{x},\tilde{t})$ (red curves), stationary thick ice (shaded), and flowing regions (arrows) at different times. The compactness evolves similarly to the thickness in both (a) and (b).

consistent with previously observed and simulated mechanisms of ice arch formation in which a polynya is formed downstream of the arch [3,25,26]. A third type of steady state occurs trivially when $\tilde{p}_i > \tilde{w}$ everywhere in the channel, for which $\langle\tilde{u}\rangle = 0$ throughout and no arch is formed. The different types of flow behavior are closely related to wave propagation in the hyperbolic system (13) and have analogies with traffic flow; these properties will be discussed elsewhere.

Thus, for a channel with maximum and minimum half-widths $w_{\max}$ and $w_{\min}$, respectively, the condition for arch formation with uniform initial ice properties is $w_{\min}/w_0 < \tilde{p}_i < w_{\max}/w_0$ or

$$\frac{\alpha w_{\min} f}{S} < h_i e^{-k(1-c_i)} < \frac{\alpha w_{\max} f}{S}, \tag{14}$$

where $h_i = \alpha w_0 f\tilde{h}_i/S$ is the dimensional initial ice thickness. The steady-state flow is arrested everywhere if $h_i e^{-k(1-c_i)} > \alpha f w_{\max}/S$, and is fully mobile if $h_i e^{-k(1-c_i)} < \alpha f w_{\min}/S$. We remark that the above predictions for the structure of the steady-state flow are independent of $\zeta_{\min}$.

We validate the predictions of our theory against direct numerical simulations of the full 2D system (1)–(5) using standard methods in sea ice modeling [20,25]. Figure 4 quantifies the structure of the steady-state flow and shows theoretical predictions (shaded areas) alongside 2D numerical simulations (symbols), indicating that either flowing, bridged, or fully arrested steady states are attained depending on the initial ice properties.

We remark that our reduced-order theory does not guarantee stability of the arch, and therefore, slightly underpredicts the minimum initial thickness required for bridge formation, cf. Fig. 4. In particular, as the ice pack opens up downstream of the initial blockage, the length scales in both the x and y directions become comparable, and the dynamics in the vicinity of the arch are fully two dimensional, see Figs. 3(b) and 3(c). Nonetheless, the present theory captures several features of the simulations and predicts realistic values of ice thickness (a few meters) for arch formation in straits with widths ~50 km and typical wind stresses [25,26], cf. Fig. 4.

The area flux of ice can be inferred from (12) as

$$q = \max\left\{\frac{2\alpha^2 w^3 f}{3\zeta_{\min}}\left[1 - \left(\frac{p}{\alpha w f}\right)^3\right], 0\right\}, \tag{15}$$

which assumes the dominance of internal stresses over water drag on the ice, and is therefore expected to be accurate for strong ice, i.e., $p/(\alpha w f) = \mathcal{O}(1)$. For relatively weak ice [$p/(\alpha w f) \ll 1$], water drag provides the main resistance to flow, balancing atmospheric stress and establishing the free-drift velocity scale $u_{\mathrm{fd}} \sim \sqrt{f/(\rho_w C_{dw})}$; here ρ_w and C_{dw} are, respectively, the density of water and the water-ice drag coefficient.

The two velocity scales become comparable when $p = \alpha w f\{1 - 3\zeta_{\min}/\sqrt{4\alpha^4 w^4 f C_{dw}\rho_w}\}^{1/3}$, setting a lower bound on p for the applicability of our theory. On the other hand, the weak-ice limit ($p \ll \alpha w f$) of (15) provides reasonable agreement with measured ice velocities in Nares Strait as a function of the wind stress [27] ($|\mathbf{u}| \lesssim 0.3\ \mathrm{m\,s^{-1}}$ for $f \lesssim 0.6$ Pa) when using the standard values of $\zeta_{\min} = 4 \times 10^8$ Pa m s and $\alpha \approx 1$ [25], see also [3,28]. A more direct quantitative comparison with

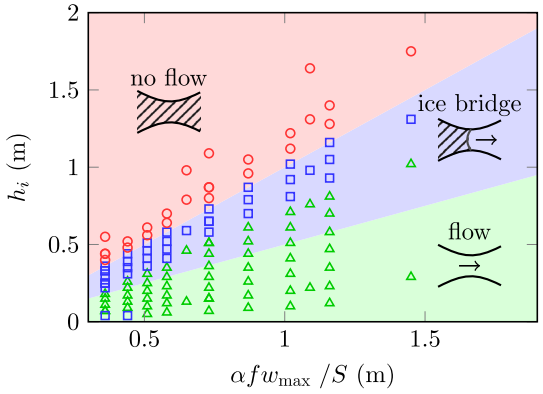

FIG. 4. Phase diagram of the steady-state flow as a function of initial ice thickness h_i (with $c_i = 1$) and the thickness scale $\alpha f w_{\max}/S$ for a channel with $w_{\min} = w_{\max}/2 = 25$ km. The reduced-order theory predicts unimpeded flow if $h_i < \alpha f w_{\min}/S$ (shaded green), fully arrested flow if $h_i > \alpha f w_{\max}/S$ (shaded red), and the formation of ice bridges for intermediate values, $\alpha f w_{\min}/S > h_i > \alpha f w_{\max}/S$ (shaded blue), with both arrested and flowing regions. Depending on the initial thickness, 2D direct numerical simulations exhibit either unimpeded flow (green triangles), arrested motion (red circles), or ice bridges (blue squares) at steady state. Here, we use the standard values of $S = 13.75$ kPa and $k = 20$ [11,25].

observations is challenging at present due to the lack of simultaneous measurements of ice properties and wind speeds in straits. We remark that the role of the limiting viscosity $\zeta_{\min}$ in the flux of sea ice is largely unappreciated and is likely to limit the sea ice export associated with the breakup of ice bridges due to the appreciable internal stresses upstream of the arch. Although it is common practice in sea ice modeling to take the limiting viscosity $\zeta_{\min}$ to be a constant independent of h or c, our results do not rely on this assumption and are more generally applicable.

Our study of ice bridges in narrow straits quantifies an important geophysical phenomenon that has consequences for both climate and ecology. We have shown that the formation of ice bridges can be understood in terms of a yield-stress mechanism and have provided quantitative predictions both for the critical ice properties for arch formation, as well as the flow rates associated with wind-driven ice motion in straits, e.g., during the breakup of such bridges. The similarity of ice arching to the jamming of dense granular flows and the behavior of yield-stress fluids suggests interesting physical and mechanistic connections between these different systems.

The authors thank J. T. Ault, D. L. Feltham, A. Muenchow and R. H. Socolow for insightful discussions and the Carbon Mitigation Initiative of Princeton University for the partial support of this research.

*hastone@princeton.edu

[1] I. Stirling, J. Mar. Syst. **10**, 9 (1997).
[2] R. F. Marsden, J. Serdula, E. Key, and P. J. Minnett, Atmos.-Ocean **42**, 251 (2004).
[3] R. Kwok, L. Toudal Pedersen, P. Gudmandsen, and S. S. Pang, Geophys. Res. Lett. **37**, L03502 (2010).
[4] J. P. Bowman and R. D. McCuaig, Appl. Environ. Microbiol. **69**, 2463 (2003).
[5] K. A. Hobson, A. Fisk, N. Karnovsky, M. Holst, J.-M. Gagnon, and M. Fortier, Deep Sea Res. Part II Top. Stud. Oceanogr. **49**, 5131 (2002).
[6] M. D. Coon, G. A. Maykut, and R. S. Pritchard, AIDJEX Bull. **24**, 1 (1974).
[7] M. Leppäranta, *The Drift of Sea Ice* (Springer Science & Business Media, Berlin, Germany, 2011).
[8] W. D. Hibler, III, J. K. Hutchings, and C. F. Ip, Annals of Glaciology **44**, 339 (2006).
[9] K. E. Trenberth, *Climate System Modeling* (Cambridge University Press, Cambridge, UK, 1992).
[10] W. D. Hibler, III, J. Geophys. Res. **82**, 3932 (1977).
[11] W. D. Hibler, III, J. Phys. Oceanogr. **9**, 815 (1979).
[12] The plastic part of the rheology follows from assuming that the plastic stresses lie on an elliptic yield curve with eccentricity α and that a normal flow rule relates stress to strain rate. The additional viscous regularization for very small strain rates in [10,11] is not important here.
[13] P. Jop, Y. Forterre, and O. Pouliquen, Nature (London) **441**, 727 (2006).
[14] Y. Forterre and O. Pouliquen, Annu. Rev. Fluid Mech. **40**, 1 (2008).
[15] D. L. Henann and K. Kamrin, Proc. Natl. Acad. Sci. U.S.A. **110**, 6730 (2013).
[16] A. S. Thorndike, D. A. Rothrock, G. A. Maykut, and R. Colony, J. Geophys. Res. **80**, 4501 (1975).
[17] S. Toppaladoddi and J. S. Wettlaufer, Phys. Rev. Lett. **115**, 148501 (2015).
[18] A. V. Wilchinsky and D. L. Feltham, J. Phys. Oceanogr. **34**, 2852 (2004).
[19] D. L. Feltham, Annu. Rev. Fluid Mech. **40**, 91 (2008).
[20] E. C. Hunke and J. K. Dukowicz, J. Phys. Oceanogr. **27**, 1849 (1997).
[21] N. J. Balmforth and R. V. Craster, J. Non-Newtonian Fluid Mech. **84**, 65 (1999).
[22] I. Frigaard and D. Ryan, J. Non-Newtonian Fluid Mech. **123**, 67 (2004).
[23] A. Harten, P. D. Lax, and B. van Leer, SIAM Rev. **25**, 35 (1983).
[24] R. J. LeVeque, *Finite Volume Methods for Hyperbolic Problems* (Cambridge University Press, Cambridge, UK, 2002), Vol. 31.
[25] D. Dumont, Y. Gratton, and T. E. Arbetter, J. Phys. Oceanogr. **39**, 1448 (2009).
[26] S. A. Stelma, Master's thesis, University of Delaware, 2015.
[27] R. M. Samelson, T. Agnew, H. Melling, and A. Münchow, Geophys. Res. Lett. **33**, L02506 (2006).
[28] R. Kwok, Geophys. Res. Lett. **33**, L16501 (2006).